communications biology

A Nature Portfolio journal

Article

https://doi.org/10.1038/s42003-026-09806-5

Early cAMP signaling orchestrates single-cell synchronicity throughout Dictyostelium development

Mariko Katoh-Kurasawa [1,5], Lena Trnovec[2,5], Peter Lehmann [1], Rui Chen[1,4], Yumei Li[1,4], Blaž Zupan [2,3] ✉ & Gad Shaulsky [1,3] ✉

Synchronicity is observed in many biological systems, including development, as seen in vertebrate body axis formation, fly eye development, and development of the social amoeba *D. discoideum*. Despite its prevalence, quantitative analyses of synchronicity at the single-cell level remain rare. Here we show that synchronicity in *D. discoideum* is mediated by early cAMP signaling. Using single-cell RNA sequencing (scRNA-seq), we quantify transcriptome similarities between individual cells during development. We show that synchronicity first declines upon starvation but then increases with the onset of cAMP-pulse signaling. Synchronicity remains stable throughout development and differs between prespore and prestalk cells. Genetic perturbations of cAMP production and response reveal that cAMP signaling is essential for establishing and maintaining synchronicity, as its absence leads to highly asynchronous development. These findings highlight the role of cAMP signaling in coordinating transcriptomic and morphological synchronicity, and establish scRNA-seq as a tool for quantitative analysis of developmental synchronicity.

Synchronicity is defined as the similarity in cell states among individual cells at given states. It is observed in many biological systems, including development where cells, tissues, and organs differentiate and undergo coordinated morphogenesis to generate properly functioning organisms. Some of the best examples of synchronicity are seen in the development of the vertebrate body axis[1] and the development of the fly eye[2]. Among protists, *Dictyostelium discoideum* is an exquisite example of synchronicity among cells, tissues, and whole organisms during development[3]. *D. discoideum* is a powerful model for studying developmental synchronicity because its transition from unicellular to multicellular development is rapid, genetically tractable, and highly coordinated across large cell populations. The cells of this social organism propagate as solitary amoebae while feeding on bacteria in the soil. When they starve, the cells aggregate to form a fruiting body consisting of a ball of spores carried atop a cellular stalk[4]. Development begins with a unicellular phase of about six hours in which the cells exhibit coordinated cringing behaviors, in which the cells alternate between rounded and polarized morphology[5], and eventually directional motility[6]. These events are synchronized by six-minute pulses of production, secretion, and response to extracellular cyclic adenosine monophosphate (cAMP), which serves as a secreted signal as well as a second messenger[7,8]. The cells aggregate by chemotaxis to cAMP from territories of about one square centimeter, three orders of magnitude larger than the footprint of a developing cell[9]. The individual aggregates, each containing roughly 100,000 cells, undergo morphogenesis, transitioning from loose aggregates to tight aggregates, fingers, migrating slugs, and culminants. They develop synchronously over distances greater than 10 cm from one another, appearing uniform in size, shape, and spatial distribution, until they form fruiting bodies after 24 h[4,6]. While the molecular mechanisms underlying *Dictyostelium* chemotaxis are well characterized[10], the processes that establish and maintain synchronicity of cell state and organismal morphology during development are largely undefined, partly due to the absence of tools for quantitative analysis of synchronicity at the single-cell resolution. In particular, it is unclear whether early signaling events mediate long-term synchronicity or if distinct synchronization mechanisms operate at different stages.

We hypothesized that cAMP-pulse signaling during early development provides sustained synchronicity throughout the process. To test this hypothesis, we used single-cell RNA sequencing (scRNA-seq) to quantify cell-state similarity across developmental time and between genetic variants. We defined synchronicity as the similarity in transcriptome profiles between individual cells. This approach is based on the observation that

[1]Department of Molecular and Human Genetics, Baylor College of Medicine, Houston, TX, USA. [2]Faculty of Computer and Information Science, University of Ljubljana, Ljubljana, Slovenia. [3]Huffington Department of Education, Innovation and Technology, Baylor College of Medicine, Houston, TX, USA. [4]Present address: Gavin Herbert Eye Institute, Center for Translational Vision Research, Department of Ophthalmology and Vision Science, University of California Irvine School of Medicine, Irvine, CA, USA. [5]These authors contributed equally: Mariko Katoh-Kurasawa, Lena Trnovec. ✉e-mail: blaz.zupan@fri.uni-lj.si; gadi@bcm.edu

Dictyostelium transcriptomes reliably represent developmental states and can be used to evaluate cellular responses to developmental, environmental, and genetic perturbations[11–17].

Temporal progression is expected to reduce overall similarity between developing cells due to the increasing differences between the cells as they differentiate. In *D. discoideum* development, cAMP-pulse signaling has profound effects on the synchronicity of cell physiology, morphology[18–20], and early gene expression[21,22], so it is expected to increase synchronicity during early stages of development. Consequently, eliminating cAMP-pulse signaling is expected to reduce synchronicity, but this inference is not straightforward. Eliminating cAMP-pulse signaling prevents developmental progression[23], so the combined effects of this perturbation on overall synchronicity are hard to predict. Regardless, we predict that inducing development despite the absence of cAMP-pulse signaling would greatly decrease synchronicity over developmental time because it combines the temporal progression in development with the absence of cAMP-pulse synchronization. To determine whether early cAMP-pulse signaling is necessary to induce and maintain transcriptomic synchronicity throughout development, we quantified cell-state similarity over time in wild-type and mutant strains using scRNA-seq. To test the hypotheses, we measured synchronicity between cells in the laboratory wild-type strain AX4 and two of its derivatives. The *acaA*$^-$ strain is incapable of cAMP-pulse signaling due to inactivation of the aggregation-stage adenylyl cyclase gene *acaA*. It is also incapable of multicellular development[23] and its transcriptome does not change much after the first four hours of development[12]. The *acaA*$^-$*pkaC*^{OE} strain is a derivative of the *acaA*$^-$ strain, in which the catalytic subunit of the cAMP-dependent protein kinase A is overexpressed. This strain is capable of development without cAMP-pulse signaling[24] and it exhibits accelerated transcriptome progression during development[12]. We used mRNA abundance profiles obtained by scRNA-seq as an indicator of cell state, and the similarity between these profiles as a measure of synchronicity between the cells.

Our results show that cAMP-pulse signaling during early development induces transcriptome synchronicity at the single-cell level and morphological synchronicity at the multicellular level. In its absence, however, synchronicity is compromised despite continued development, indicating that early signaling events are required for synchronous developmental progression.

Results

Morphological synchronicity emerges early during wild-type development but is lost when cAMP signaling is disrupted

To test the level of intercellular synchronicity during development, we first developed cells by depositing them on black nitrocellulose filters in non-nutrient buffer. This procedure induces synchronous morphogenesis in AX4 cells as seen in Fig. 1. After eight hours of development, the AX4 cells appeared as loose aggregates with minor variations in shape, size, and spatial distribution. Each aggregate contains about 10^5 cells[9]. At 12 h, the cells appeared as tipped aggregates of similar shape, size, and distribution. The anterior tip regions consist of prestalk cells and the posterior regions contain mainly prespore cells and a few anterior-like prestalk cells[25,26]. At 16 h, the cells appeared as fingers and slugs that are about 1–2 mm long, and at 20 h they became culminants, with the beginnings of stalks protruding from the bases of the aggregates (Fig. 1). We did not allow the cells to complete the developmental process because extraction of mRNA from spores and stalks is inconsistent with the scRNA-seq procedure we used, but at 24 h the developmental structures are mainly fruiting bodies with a ball of spores carried atop a cellular stalk[6]. The *acaA*$^-$ cells failed to aggregate altogether, so their photographs in Fig. 1 appear featureless as expected. The *acaA*$^-$*pkaC*^{OE} cells appeared unaggregated at eight hours (Fig. 1). At 12 h, they appeared as a mix of mostly loose aggregates and some tight aggregates which were smaller than the AX4 aggregates but rather uniform in shape, size, and spatial distribution. At 16 and 20 h, the *acaA*$^-$*pkaC*^{OE} cells appeared as mixes of several stages, including loose aggregates, tight aggregates, tipped aggregates, fingers/slugs, and culminants (Fig. 1). This lack of morphological synchronicity was not reported in the original study of the *acaA*$^-$*pkaC*^{OE} cells[24], but it was documented in later studies[12]. Analyses of these strains by standard RNA-seq showed that *acaA*$^-$ cells fail to express developmental genes, whereas the *acaA*$^-$*pkaC*^{OE} cells develop more rapidly than the AX4 cells during the starvation stage but then appear to develop more slowly during the multicellular stages[12].

Cell synchronicity dynamics during wild-type development

To test the degree of cell population synchronicity during development we collected cells at the onset of starvation (0 h) and at four-hour intervals for 20 h of development. We processed the cells with scRNA-seq and embedded their transcriptomes into a reduced, 1280-dimensional space using the universal cell embedding (UCE) foundation model[27]. We computed synchronicity as a normalized similarity score (ranging between 0 and 1) based on pairwise distances between L2-normalized cell embeddings at each time point. Higher scores indicate greater similarity among cells and thus higher synchronicity. The validity of this reasoning has been demonstrated in scRNA-seq analysis of cells during aging[28,29]. We used three or four independent replicates at each time point and calculated their means to evaluate the differences between the samples across time points and genotypes.

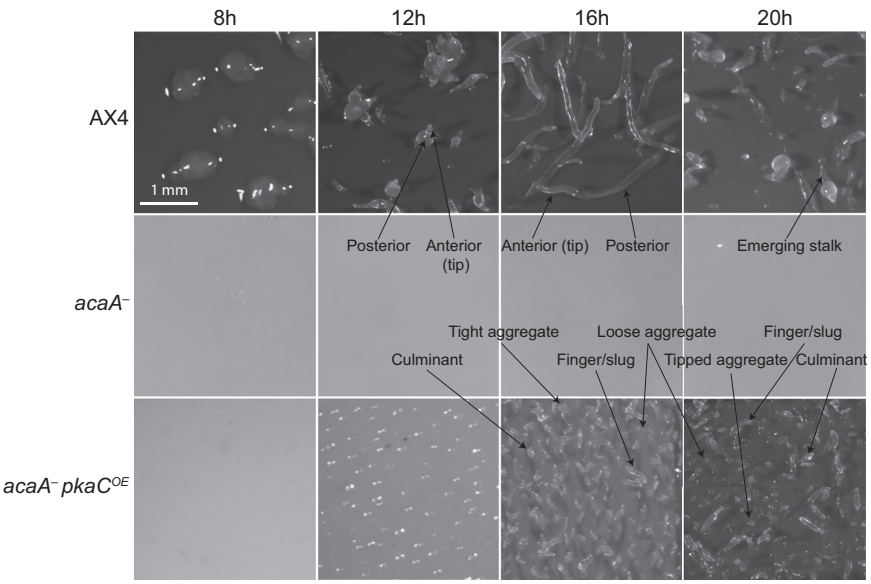

Fig. 1 | Morphological synchronicity emerges early during wild-type development but is lost without cAMP-pulse signaling. We developed cells and photographed the multicellular structures from above through a dissecting microscope. The strain names are indicated on the left of each row, and the developmental times (hours) are indicated above each column. The size bar in the upper left image applies to all the panels. AX4: 8 h – loose aggregates; 12 h – tipped aggregates with posterior and anterior (tip) regions indicated on one of the structures (arrows); 16 h – fingers/slugs with posterior and anterior (tip) regions indicated on one of the structures (arrows); 20 h – fingers and culminants with emerging stalks as indicated on one of the structures (arrow). *acaA*$^-$: these cells did not aggregate at all. *acaA*$^-$*pkaC*^{OE}: 8 h – no aggregates; 12 h – loose aggregates; 16 h and 20 h – a mix of loose aggregates, tight aggregates, tipped aggregates, fingers/slugs, and culminants, as indicated by arrows.

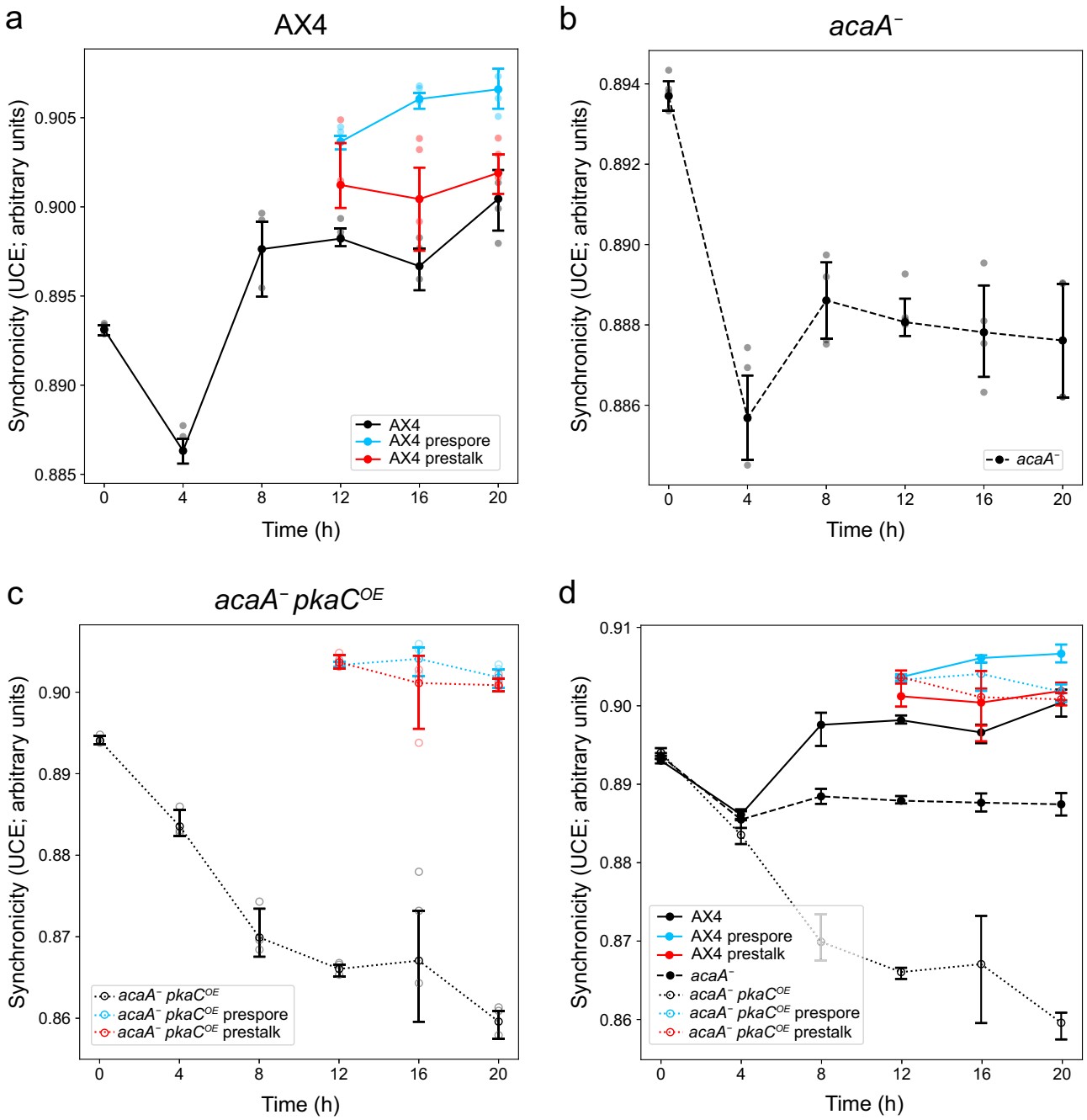

Fig. 2 | Cell synchronicity dynamics during development reveal the essential role of early cAMP-pulse signaling. We developed cells, collected samples at four-hour intervals between the onset of starvation (0 h) and 20 h, performed scRNA-seq analysis, and computed the synchronicity of the cell population using the UCE embeddings. We plotted synchronicity (UCE; arbitrary units, y-axis) against developmental time (hours, x-axis) for the entire cell population (black symbols and lines) throughout the time course, and also separately for prespore cells (cyan) and prestalk cells (red) at 12–20 h. Each dark point in the graphs shows the mean of the replicates (three independent replicates for AX4 and *acaA*⁻*pkaC*^{OE}; four independent replicates for *acaA*⁻). The error bars indicate 95% bootstrap confidence intervals (2.5th–97.5th percentiles). Points shown at 50% opacity represent the respective independent replicates. **a** AX4; (**b**) *acaA*⁻; (**c**) *acaA*⁻*pkaC*^{OE}; (**d**) the three strains together. The y-axes are different between (**d**–**g**). Graphs describing the individual replicates are also provided in Supplementary Fig. 2. Statistical significance (t-test) of comparisons between all the strains, time points, and cell types are provided in Supplementary Tables 1, 2, and 3. Numerical source data are provided in Supplementary Data 1 and Supplementary Data 3.

Figure 2a and Supplementary Data 1 shows that AX4 cell synchronicity decreased markedly during starvation, between 0 and 4 h. This decrease is consistent with the knowledge that starvation introduces an environmental change that affects the transcriptome, and there is no known mechanism that synchronizes the cells during that process[13,14]. The magnitude of the change was rather large – it was the second largest change in the entire AX4 time course. Synchronicity increased between 4 and 8 h, and that change was the largest in the AX4 time course (Fig. 2a). This increase coincides with the establishment of extracellular cAMP-pulse signaling and the beginning of the transition from unicellular behavior to multicellular development[12]. This large increase in synchronicity, and the established roles of cAMP-pulse signaling in *Dictyostelium* development, suggest that transcriptome synchronicity at the single-cell level is also mediated by cAMP-pulse signaling. Synchronicity remained high throughout the rest of development

with minor fluctuations (Fig. 2a). The differences between the 0 h, 4 h, and 8 h time points were statistically significant (Supplementary Table 1). The synchronicity levels during the rest of development were not significantly different from one another, but significantly different from the 0 h and 4 h time points (Supplementary Table 1).

The stability of synchronicity during the multicellular stages, between 8 and 20 h, can be interpreted in several ways. The simplest explanation is that the initial synchronization process is sufficient to induce stable synchronicity, but this possibility does not explain why differentiation into the prespore and prestalk cell types and subtypes did not reduce overall synchronicity after 12 h. An alternative explanation is that the differentiation into prespore and prestalk cells causes a decrease in synchronicity that is not large enough to reduce the overall synchronicity. To test that possibility, we used prespore and prestalk markers to identify the two cell types in the 12 h, 16 h, and 20 h time points. Figure 2a shows that prespore (cyan) and prestalk (red) cells appear to be more synchronous than the total cell population (black), and Supplementary Table 2 shows that the differences are significant in most time points. This observation suggests that the differences between prespore and prestalk cells reduce the combined synchronicity of the cell population, but not enough to affect the overall synchronicity pattern. Figure 2a and Supplementary Table 2 also show that prespore cells are more synchronous than prestalk cells. This finding is consistent with previous observations that prestalk cells consist of several subtypes whereas prespore cells are more homogeneous[25,30]. The consistency of these findings with published work supports the idea that scRNA-seq data accurately represent cell synchronicity.

Cell-synchronicity in mutant strains reveals the essential role of early cAMP-pulse signaling

We then tested the synchronicity of cells that lack cAMP-pulse signaling due to elimination of the *acaA* gene. Figure 2b shows that *acaA*$^-$ cell synchronicity decreased markedly in the first four hours after starvation. Comparing the synchronicity levels at 0 h and 4 h revealed that the decrease was large and statistically significant (Supplementary Table 1). We also observed a small increase in synchronicity between 4 h and 8 h, which was statistically significant and somewhat surprising (Fig. 2b). We expected that without the synchronizing effects of cAMP pulses, the cells would continue to accumulate changes, which would reduce synchronicity further. The increase in synchronicity between 4 and 8 h in *acaA*$^-$ suggests that the starved cells have a limited physiological repertoire that is less variable than the initial starvation process. The synchronicity levels declined somewhat between 8 and 20 h (Fig. 2b), which was consistent with our prediction, but these changes were not statistically significant (Supplementary Table 1). The *acaA*$^-$ cells do not develop into prespore and prestalk cells, so we did not analyze the synchronicity within and between these cell types.

In the third set of experiments, we examined the impact of development without cAMP-pulse signaling on synchronicity, using *acaA*$^-$*pkaC*^{OE} cells in which overexpression of the PKA catalytic subunit restores multicellular development[24]. The *acaA*$^-$*pkaC*^{OE} cell synchronicity decreased during development, with a marked decline during the first eight hours and another decline between 16 and 20 h (Fig. 2c and Supplementary Table 1). The decrease in synchronicity throughout most of the time course is consistent with the hypothesis that cAMP-pulse signaling is the major synchronizing factor in *D. discoideum* development. In the *acaA*$^-$*pkaC*^{OE} cells, prespore and prestalk synchronicities were significantly higher than the total, but not significantly different from one another (Fig. 2c and Supplementary Table 3).

The analyses in Fig. 2a–c were done by comparing different time points within each strain. The temporal changes in synchronicity were largely consistent with the hypothesis that development and differentiation reduce synchronicity whereas cAMP-pulse signaling increases it. To determine the effects of the genetic perturbations, we compared the synchronicity trajectories of the three strains in one graph (Fig. 2d and Supplementary Table 1). We found that the three strains exhibited the same level of synchronicity before the onset of development (Fig. 2d and Supplementary Table 1, 0 h). This result is consistent with the facts that the cells were grown under identical conditions and the genetic perturbations do not affect growth[12,23,24]. It further validates the experimental approach and the idea that scRNA-seq profiles are suitable measures of synchronicity. Comparing the strains between 0 and 4 h showed that all three strains exhibited a significant and nearly identical decrease in synchronicity upon starvation. (Fig. 2d and Supplementary Table 1). Comparing AX4 and *acaA*$^-$ at 8 h shows that the increased synchronicity in *acaA*$^-$ was significantly smaller than the one observed in AX4 (Fig. 2d and Supplementary Table 1, 8h). Synchronicity remained lower in *acaA*$^-$ compared to AX4 for the rest of the time course with minor fluctuations that were not statistically significant. This finding suggests that the absence of cAMP-pulse signaling prevents the cells from gaining synchronicity, but it does not directly implicate cAMP-pulse signaling as the causative factor because the *acaA*$^-$ cells do not develop. The needed support for that hypothesis comes from the comparison to the *acaA*$^-$*pkaC*^{OE} cells. These cells aggregate by accretion in the absence of cAMP-pulse signals and develop into prespore and prestalk cells with compromised morphological synchronicity[12,24]. The data in Fig. 2d show that *acaA*$^-$*pkaC*^{OE} cells exhibit a large decrease in synchronicity compared to AX4 and *acaA*$^-$ and the differences are statistically significant at every time point after 4 h (Supplementary Table 1). Comparing the prespore and prestalk subpopulations (Fig. 2d and Supplementary Tables 2 and 3) shows that the prespore and prestalk cells of the *acaA*$^-$*pkaC*^{OE} strain were roughly as synchronous as their AX4 counterparts.

UCE is a foundation model that was trained on diverse single-cell datasets and includes biological priors that make it especially suitable for this data set[27]. Because UCE has not been tested on *Dictyostelium* datasets before, we repeated the synchronicity analysis with Principal Component Analysis (PCA) for added confidence. Unlike UCE, PCA is a purely data-driven, linear dimensionality reduction method that lacks biological priors and is therefore expected to capture only dominant sources of variance rather than finer, biologically meaningful structure. The inferred synchronicity trends shown in Supplementary Fig. 1 and Supplementary Data 2 are largely similar to those shown in Fig. 2. In the case of AX4 cells (Supplementary Fig. 1a), the PCA-based analysis revealed a large drop in synchronicity at 4 h, a large increase in synchronicity at 8 h, and a subsequent reduction in synchronicity at 12 h and 16 h. These observations concur with the trends shown in Fig. 2a, although the magnitude of the changes is somewhat different. Likewise, the prespore synchronicity measured with the PCA-based values was larger than the total cell population synchronicity, and the prespore cells appeared more synchronized than the prestalk cells (Supplementary Fig. 1a), as seen with the UCE-based analysis (Fig. 2a). However, the PCA analysis did not capture the expected difference in synchronicity between the prestalk cells and the total population, consistent with its reduced sensitivity to subtler biological distinctions. The trend found with the PCA-based analyses of the *acaA*$^-$ cells (Supplementary Fig. 1b) was similar to that found with the UCE-based analysis of the same strain (Fig. 2b), with a large drop in synchronicity during the first 4 h and minor fluctuations thereafter. In the *acaA*$^-$*pkaC*^{OE} cells (Supplementary Fig. 1c) we observed trends that were largely similar to those found with the UCE-based analysis as well (Fig. 2c). Here, we found a consistent decline in synchronicity throughout the developmental time course, although the PCA-based analysis showed a sharper drop during the first 4 h than the UCE-based analysis. The prespore and prestalk cell synchronicity was also higher than the synchronicity of the total population, and the prespore cells seemed slightly more synchronous than the prestalk cells (Supplementary Fig. 1c) compared to the near-equal levels seen with the UCE based method (Fig. 2c). Moreover, comparing the PCA-based synchronicity trajectories of the three strains and the respective cell types in one graph (Supplementary Fig. 1d) yielded similar trends to those seen with the UCE-based analysis (Fig. 2d). The ability of PCA to reproduce the dominant global trends, despite its methodological limitations, supports the robustness of the results, while the additional structure captured by UCE underscores its superior suitability for quantitative analysis of developmental synchronicity in this system. We therefore conclude that the UCE method is indeed suitable for this analysis.

Overall, the data in Fig. 2 and Supplementary Fig. 1 support the hypothesis that cAMP pulse signaling during early development sets the cells on a path toward synchronous development. By definition, cell-type differentiation is a process that reduces synchronicity, but the differences between the prespore and prestalk transcriptomes are not large enough to reduce the apparent synchronicity of the entire cell population. The data also suggest that starvation without development slightly synchronizes the cells independently of cAMP-pulse signaling.

Many scRNA-seq analyses of developmental systems utilize internal replication at the single-cell level to draw conclusions about the differences between cell types. However, our experimental approach was different, requiring replication through repeating the time-course experiments. To reduce cost, we used a tagging system that enabled pooling of samples from independent biological replicates and processing them together through the scRNA-seq protocol. We generated three strains of AX4 that were transformed with constructs to express the fluorescent proteins GFP, mCerulean, or mCherry under control of the actin15 promoter. We grew and developed the cells separately, and pooled them just before the scRNA-seq procedure. During data analysis, we identified differentially tagged cells as those that exhibited mRNA sequences from the respective transgenes. For *acaA*$^{-}$ we generated four strains, adding mNeonGreen to the aforementioned tags. Generating tags in the *acaA*$^{-}$*pkaC*^{OE} background was complicated, so we used only one strain with three independent replications, including independent scRNA-seq processing. Supplementary Fig. 2a and Supplementary Data 3 show results from the different replicates in different colors and the population averages in black. The general trends of the replicates in Supplementary Fig. 2a are very similar to the mean trends, suggesting agreement between the replicates. We also noticed that the independent replicates of the *acaA*$^{-}$*pkaC*^{OE} strain were more similar to one another than the replicates of the other two strains (Supplementary Fig. 2a).

Temporal developmental progression is disrupted without cAMP-pulse signaling

To further validate the experimental approach and the results, we examined the temporal resolution in the data by generating two dimensional UMAP representations of the UCE transcriptome embeddings. Figure 3a shows the results for AX4, where data points were colored based on the sampling time point and Fig. 4 shows the same data in separate panels for the different time points. We observed that the cells were represented in two major clusters (Fig. 3a). The cluster on the right represents mainly cells collected at 0 h and

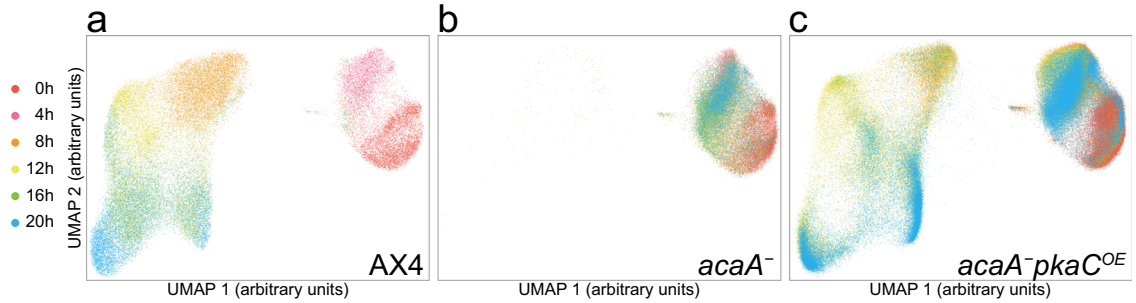

Fig. 3 | Temporal developmental progression is disrupted without cAMP-pulse signaling. We generated a UMAP representation of individual cells in AX4 (**a**) and mapped the data from the other two strains to the pre-trained UMAP model of AX4. **b** *acaA*$^{-}$; (**c**) *acaA*$^{-}$*pkaC*^{OE}. Each point in the plots represents a cell and the point color represents the developmental time as indicated in the legend on the left. The x- and y-axes represent UMAP1 and UMAP2, respectively, in arbitrary units, as indicated. The strain names are indicated inside the panels. The data include all the replicates.

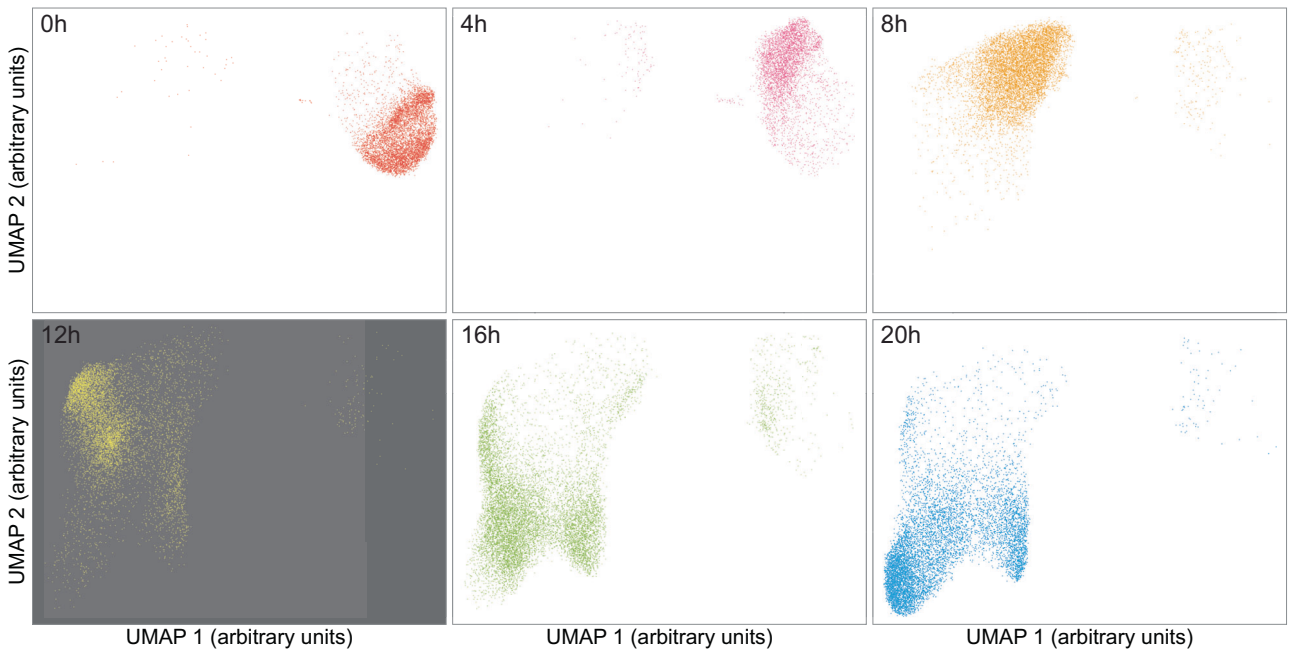

Fig. 4 | Temporal developmental progression of AX4. We generated UMAP representations of the individual cells in AX4 at the separate developmental time points as indicated inside each panel. Each point in the plot represents a cell and the color represents the developmental time, which matches the merged image shown in Fig. 3a. The 12 h panel is shown over a dark background for better contrast. The x- and y-axes represent UMAP1 and UMAP2, respectively, in arbitrary units, as indicated.

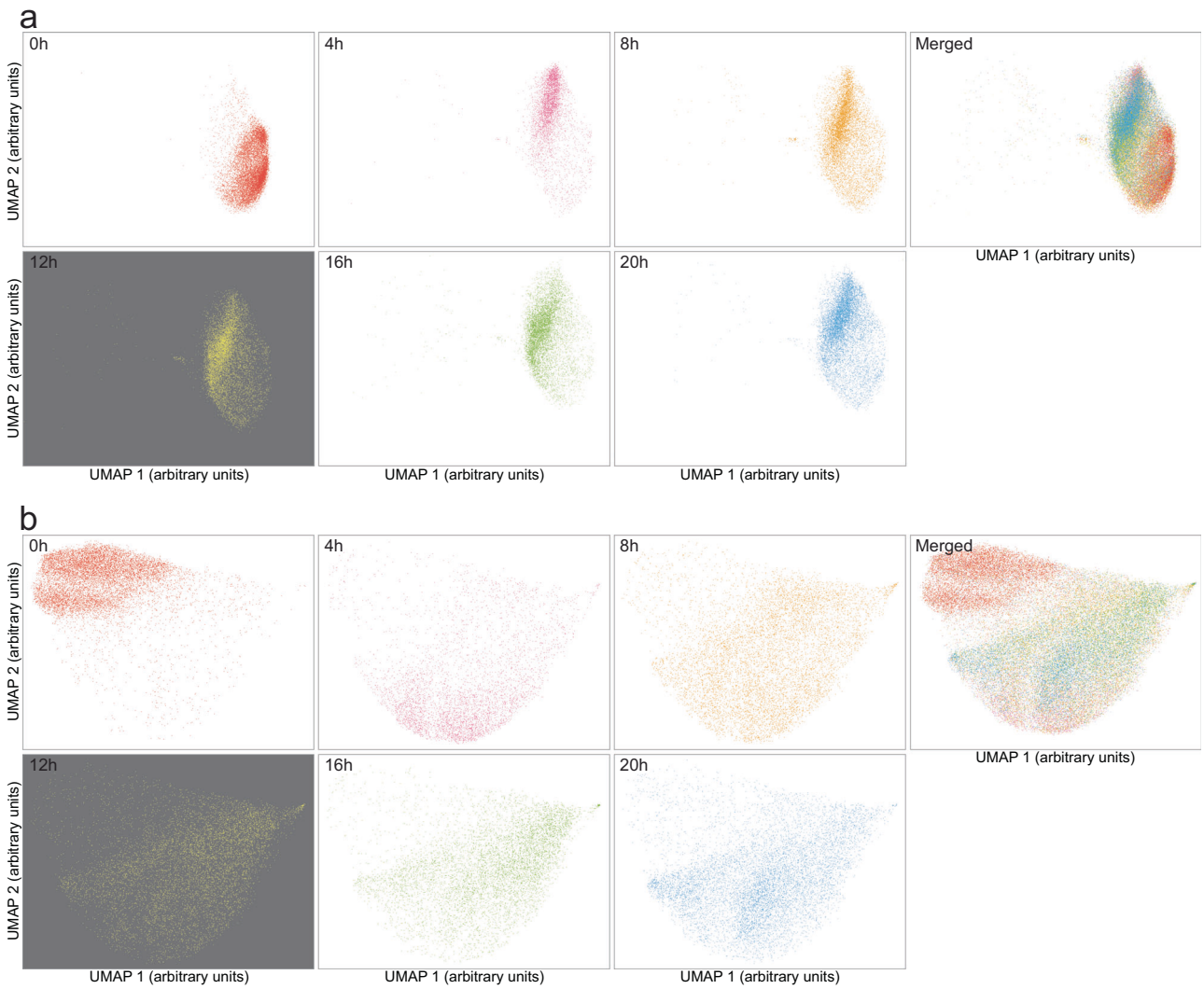

Fig. 5 | Temporal developmental progression of *acaA*⁻. We generated UMAP representations of the individual cells in *acaA*⁻ at the separate developmental time points as indicated in each panel. We mapped the data to the pretrained UMAP model of AX4 (**a**) which matches the merged image shown in Fig. 3b. We also generated separate UMAP representations without mapping to AX4 (**b**), including the merged images as indicated. Each point in the plot represents a cell, and the color of the point represents the developmental time as indicated. The 12 h panels are shown against a dark background for better contrast. The x- and y-axes represent UMAP1 and UMAP2, respectively, in arbitrary units, as indicated.

4 h, and the other cluster includes all the later time points. There was almost no overlap between the 0 h, 4 h, and 8 h cells, which is consistent with observations from standard RNA-seq, from morphological and physiological data[12–14], and from earlier scRNA-seq analyses[17]. In subsequent time points we observed some overlap between data from different times, but a clear temporal progression from the top of the image (8 h) to the bottom (20 h) (Figs. 3 and 4). These results suggest that the UCE analysis preserved the biological differences between the developmental stages, further validating the experimental approach. We also generated UMAP images in which we colored the data points based on the tags used to identify the replicate experiments (Supplementary Fig. 2b). These data show that tagging did not alter the cell profiles because the tagged cells were evenly represented in all the clusters. The density of the data points presented in the UMAP images does not match the degree of synchronicity described in Fig. 2. This observation is somewhat counterintuitive, but it should not be surprising. The UMAP algorithm is a qualitative visual tool that preserves and augments local similarities between cells. It represents relative neighborhood structures well, but may not reflect global structures[31,32]. Therefore, it is not surprising that the density of the points in the UMAP plots do not correlate with the pairwise distances we used to describe synchronicity.

To facilitate comparison between the strains, we mapped the *acaA*⁻ data to the pre-trained UMAP model of AX4. Figure 3b shows that the *acaA*⁻ data mapped mainly to the right cluster, representing the unaggregated AX4 cells. The vegetative *acaA*⁻ cells (0 h) data mapped to the same region as the vegetative AX4 cells. The other time points appeared concentrated around the 4 h cluster of AX4, with some dispersion, and almost none were mapped to the left AX4 cluster (Fig. 3b). These findings are consistent with the inability of *acaA*⁻ cells to aggregate[23], with standard RNA-seq data showing the lack of transcriptional progression past starvation[12], and with optogenetics data showing that cAMP-pulse signaling can restore transcriptional progression in an acaA-deficient mutant[17]. Figure 5a shows the *acaA*⁻ data in separate panels for each time point. We also generated UMAP images for *acaA*⁻ without mapping to the AX4 model (Fig. 5b). These data also demonstrate differences between the 0 h cells and all the others. Plotting the latter image with tagging information instead of time (Supplementary Fig. 2b) further demonstrates that tagging did not alter the cell profiles because the tags were evenly distributed across all clusters.

Mapping the *acaA*⁻*pkaC*^{OE} data onto the AX4 model revealed that the cells were represented in both clusters. This finding suggests that the cells can differentiate into all wild-type stages (Fig. 3c). The vegetative

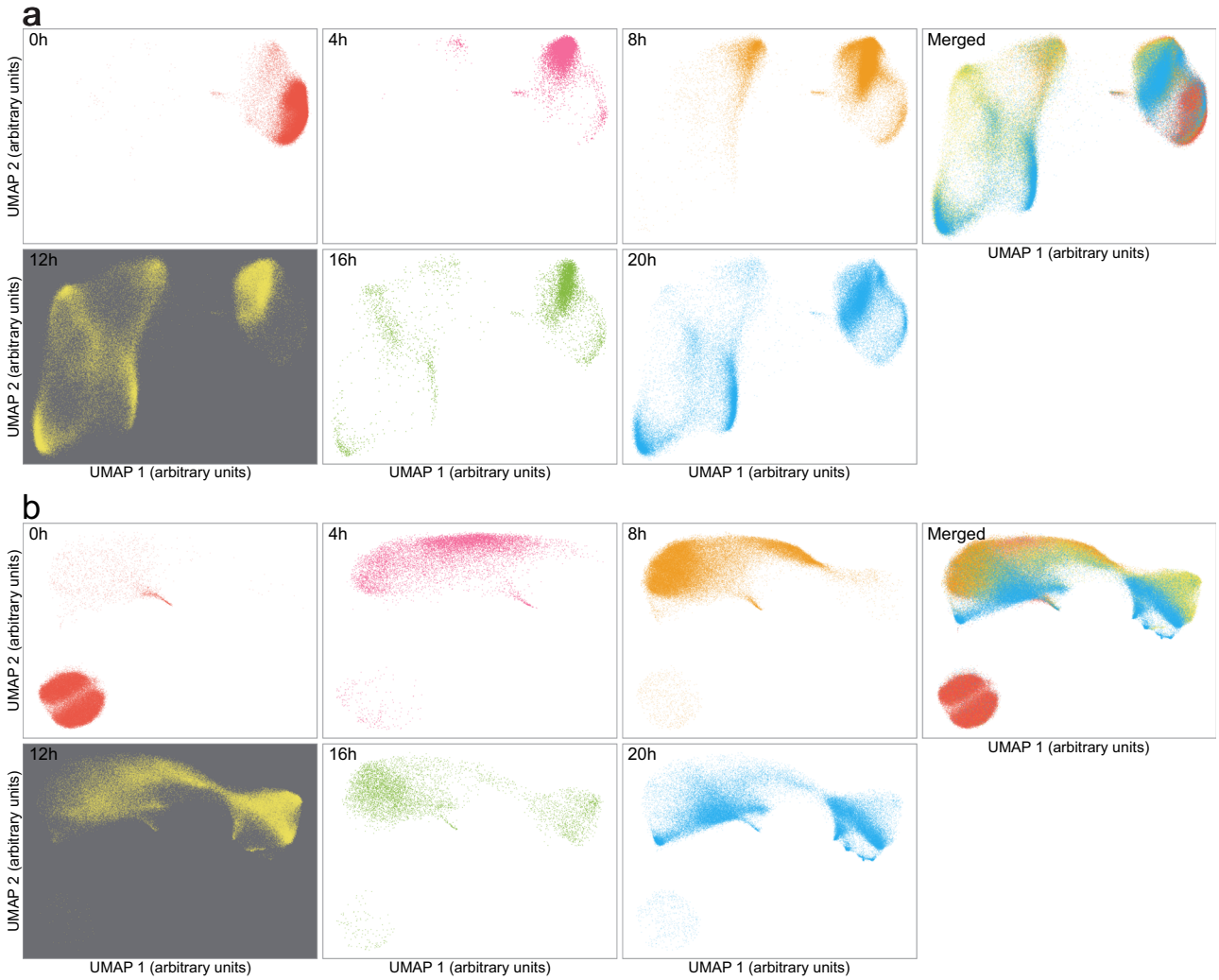

Fig. 6 | Temporal developmental progression of *acaA*$^{-}$*pkaC*^{OE}. We generated UMAP representations of the individual cells in *acaA*$^{-}$*pkaC*^{OE} at the separate developmental time points as indicated inside each panel. We mapped the data to the pre-trained UMAP model of AX4 (**a**) which matches the merged image shown in Fig. 3c. We also generated separate UMAP representations without mapping to AX4 (**b**), including the merged images as indicated. Each point in the plot represents a cell and the color of each point represents the developmental time as indicated. The 12 h panels are shown against a dark background for better contrast. The x- and y-axes represent UMAP1 and UMAP2, respectively, in arbitrary units, as indicated.

cells (0 h) were found in the same cluster as the AX4 vegetative cells and were distinct from all the other time points, showing a minor overlap with the early starving cells (4 h) (Figs. 3c and 6a). Nevertheless, the compromised synchronicity was evident. All the other time points were represented in the cluster that contains the single-cell stages of AX4, and there were major overlaps between the 8 h, 12 h, 16 h, and 20 h time points in both clusters. The precocious development of the *acaA*$^{-}$*pkaC*^{OE} cells was also evident in that some 4 h cells overlapped with the 8 h cluster of AX4, and the 12 h and 16 h cells of the *acaA*$^{-}$*pkaC*^{OE} overlapped with the 20 h cluster of AX4 (Figs. 3c and 6a). These observations are consistent with the hypothesis that *pkaC* overexpression in *acaA*$^{-}$ cells restores development but with compromised synchronicity. Generating a separate UMAP representation of the *acaA*$^{-}$*pkaC*^{OE} data without mapping to the AX4 model further supports these conclusions (Fig. 6b). In this case, the 0 h cells mainly clustered away from the rest of the time points, and there were major overlaps between the 4 h and 8 h clusters, and between the 12 h, 16 h, and 20 h clusters. Additionally, plotting the latter image with replication information instead of time (Supplementary Fig. 2b) shows that the replicates were consistent with one another because they were evenly represented in all the clusters.

Cell-type divergence during development is preserved without cAMP-pulse signaling

The UMAP representations of the late-stage AX4 cells were split into two lobes that represented mainly 16 h and 20 h cells (Fig. 3a). We suspected that these lobes represented prespore and prestalk cells. To test that possibility, we defined cells as prespore or prestalk based on the abundance of cell-type specific transcripts previously confirmed by RNA in-situ hybridization[30] and by physical separation of developing cells and standard RNA-seq analysis[13]. The results show that AX4 cells diverge into prespore and prestalk cells starting roughly at 12 h and become increasingly distinct as development progresses over time (Fig. 7). The cluster representing single AX4 cells at 0 h and 4 h was largely devoid of prespore and prestalk markers. The cluster representing aggregated AX4 cells contained mainly undifferentiated cells in the 8 h region. Regions representing cells at 12 h, 16 h and 20 h were split into prespore cells on the left and prestalk cells on the right, with little overlap between them as seen in the merged image and in the images that represent the two cell types separately.

We also examined the differentiation and distribution of the two cell types in the *acaA*$^{-}$*pkaC*^{OE} data (Fig. 7). In this case, we observed divergence into prespore and prestalk cells, largely along the same distinctions as AX4, despite the lack of synchronicity. This finding is quite significant

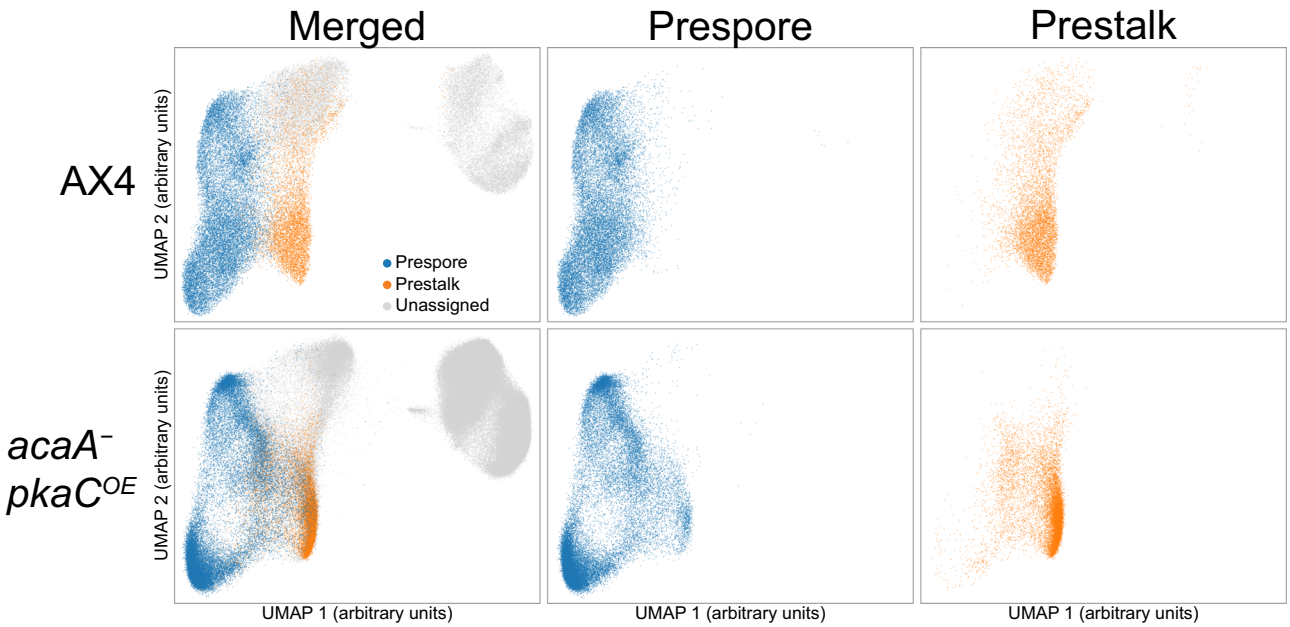

Fig. 7 | Cell-type divergence during development is preserved without cAMP-pulse signaling. We generated a UMAP representation of the individual cells in AX4 (upper panels) and mapped the *acaA*⁻*pkaC*^{OE} cell data to the pre-trained UMAP model of AX4 (lower panels). Each point in the plot represents a cell. We designated the cells as prespore (blue), prestalk (orange), or unassigned (gray), according to their gene expression profiles. Supplementary Table 4 shows the prespore and prestalk genes used for the designation. The images show the merged designations as well as the separate prespore and prestalk designations as indicated above each image. The strain names are indicated on the left of each row. The x- and y- axes represent UMAP1 and UMAP2, respectively, in arbitrary units, as indicated.

because it shows that the mutant strain development is largely restored to the AX4 pattern rather than occurring through an alternative developmental pathway. Thus, the compromised synchronicity in this strain only affects cell state over time, without compromising developmental fates.

Discussion

The data presented here support the hypothesis that transcriptome synchronicity at the single-cell level is achieved by cAMP-pulse signaling. This conclusion is based on the correlation between the time at which synchronicity is markedly increased and the time of cAMP-pulse signaling onset, between four and eight hours of wild-type development. This correlation is further supported by the reduced synchronicity observed in the *acaA*⁻ strain, which is incapable of cAMP-pulse signaling, but this argument is incomplete because the *acaA*⁻ strain is also incapable of multicellular development. Observing a large synchronicity reduction in the *acaA*⁻*pkaC*^{OE} strain completes the argument because this mutant strain develops in the absence of cAMP-pulse signaling. These data also suggest that morphological synchronicity at the multicellular-structure level is driven by the same mechanism. This conclusion is supported by the correlation between multicellular structure synchronicity and single-cell transcriptional synchronicity when comparing the three strains. In addition, there is no obvious multicellular-structure synchronicity in the *acaA*⁻*pkaC*^{OE} strain even though it undergoes morphological progression during development. These observations suggest that cAMP-pulse signaling is a major contributor to developmental synchronicity, although additional mechanisms may also play supporting roles, particularly at later developmental stages. In addition, the low synchronicity we observed in vegetative and early starved cells may reflect an underlying mechanism of stochastic gene expression. Analysis of developmental lineages and cell-type proportioning showed that genes associated with cell-type differentiation exhibit elevated cell-to-cell variability in vegetative *Dictyostelium* cells and this variability is modulated by Set1-dependent H3K4 methylation[33]. This transcriptional heterogeneity likely contributes to the reduced synchronicity we observed prior to the onset of cAMP-pulse signaling. The subsequent increase in synchronicity between four and eight hours therefore represents a transition from a transcriptionally heterogeneous baseline to a more coordinated developmental program.

Previous studies have shown that cAMP-pulses regulate gene expression. Starvation of *D. discoideum* cells in suspension with artificial cAMP pulses induces the expression of several early developmental genes in a manner that implies coordination and synchronicity[14,34]. However, these observations were made with bulk-transcriptome analysis so the cellular level of synchronicity was largely an inference. More direct evidence of cell-level synchronicity comes from the synchronous nucleus-cytoplasm shuttling of the transcription factors Hbx5 and GtaC in response to cAMP-pulse signaling. These shuttling transcription factors are also required for cAMP-pulse induced gene expression and subsequent development, suggesting that they are directly involved in the cell-level transcriptome synchronicity we observed[21,22]. Another body of evidence, based on scRNA-seq studies, has shown strong correlations between cAMP-pulse signaling and developmental fate choice, transcriptional oscillations, and collective signaling[11,17,35]. The long-term synchronicity observed in both single-cell transcriptomic profiles and multicellular morphology is likely a downstream consequence of the short-term synchronicity established by early cAMP-pulse signaling during the transition from unicellular to multicellular development. We propose this mechanism mainly because *D. discoideum* cells complete their development rapidly, only 16–20 h after the onset of cAMP-pulse signaling[6]. Moreover, these amoebae develop without replicative cell division[36,37], which would otherwise reduce cell synchronicity over developmental time. Furthermore, all strains were grown and developed under identical conditions to minimize differences in metabolic state.

Evidence for cAMP-pulse signaling at later developmental stages includes descriptions of coordinated cell-shape changes and oscillations of intracellular cAMP levels in multicellular structures[20,38]. However, there is also evidence that the cells lose cAMP responsiveness shortly after completing the aggregation phase, and that cAMP-pulse signaling is dispensable for post-aggregative synchronous development[39,40]. Therefore, the role of cAMP-pulse signaling in synchronizing development after the completion of aggregation is probably minimal. While we propose that the early-stage cAMP-pulse signaling mechanism explains the long-term synchronicity between cells and between multicellular structures, there is also evidence for

other synchronization mechanisms during late development. The membrane proteins TgrB1 and TgrC1 play an important role in the transition from unicellular behavior to multicellular development. They appear to replace cAMP-pulse signaling in coordinating cell movement during late stages of aggregation[40,41]. Shortly after aggregation, the soluble factor DIF-1 is produced by prespore cells and mediates the differentiation of a prestalk-cell subpopulation[42,43]. Later in development, the prestalk cells differentiate into stalk cells while descending through the prespore cell mass. At that time, they produce signals that induce gene expression and facilitate the differentiation of prespore cells into spores, progressing from the top of the fruiting body downwards[44,45]. At the same time, the anterior prestalk cells produce and secrete cyclic di-GMP, another soluble signal that promotes stalk-cell differentiation[46]. These coordinated processes synchronize the terminal differentiation of both cell types during culmination, but they are limited to individual organisms. Multicellular structures also produce volatile substances, including ammonia[47,48] and various terpenes[49–51]. These volatiles could potentially serve as synchronization factors between organisms, but there is no empirical evidence for such roles. We propose that these later signaling events occur synchronously mainly because of the early synchronizing effects of cAMP-pulse signaling and not due to other synchronization mechanisms.

Overexpression of the *pkaC* gene in the *acaA*$^-$ mutant causes suppression of the early aggregation defect, which allows the cells to develop without cAMP-pulse signaling[24]. Because *pkaC* is a key component of developmental regulation[52], it probably activates some of the late synchronization mechanisms, which function within the aggregates, without activating the cAMP-pulse signals. This might be the reason we observed synchronization within the multicellular structures of the *acaA*$^-$*pkaC*^{OE} strains but not between them. A study that used an optogenetic approach to generate cAMP pulses demonstrated coupling between development and gene expression[17], further supporting the idea that early cAMP-pulse signaling coordinates synchronous development. The uncoupling of cAMP-pulse signaling from subsequent development in the *acaA*$^-$*pkaC*^{OE} strain was therefore essential for demonstrating that development without these signals is asynchronous.

Developmental synchronization through cAMP-pulse signaling is unique to Group 4 of the Dictyostelia, which includes *D. discoideum*[53], but it is similar in principle to other developmental synchronization mechanisms. The vertebrate body axis develops under the control of a segmentation clock that utilizes Fibroblast Growth Factors, Wnt proteins, and Retinoic Acid as soluble signals that regulate long-range oscillatory signaling[1]. Another synchronized developmental pathway involves the progression of the morphogenetic furrow during *Drosophila* eye development. This process involves soluble activators and inhibitors that act at various ranges, including Hedgehog, Decapentaplegic, Wingless, Argos, and Spitz[54]. Thus, soluble factors and, in some systems, oscillatory signaling, are features associated with developmental synchronization. Additionally, both the vertebrate body axis development and the *Drosophila* morphogenetic furrow progression involve short-range signaling through membrane-bound ligands and receptors. In the two metazoan examples, Delta and Notch are involved[1,54]. We propose that the membrane bound TgrB1 and TgrC1 may serve an analogous role in *D. discoideum* to that of Delta and Notch in metazoans, mediating short-range signaling during the transition to multicellular development[41,55]. It is worth noting in this context that the scRNA-seq analysis does not distinguish between synchronicity of cells within a single multicellular organism and synchronicity between different multicellular organisms.

In addition to addressing the issue of synchronous development, our experiments have shown that collecting samples every four hours provides sufficient temporal resolution to analyze single-cell behavior during development. Unlike many other scRNA-seq experiments, we did not use pseudo-time analysis to infer temporal progression during development. Moreover, the UCE foundation model[27] appeared to preserve biologically meaningful structure in the data, as it produced the expected distinction between the early single-cell stage (0 h and 4 h) and the later multicellular stages (8 h to 20 h). It also retained the temporal progression of the developmental stages, as seen in the UMAP representations. This finding is notable considering that the UCE model training did not include *D. discoideum* data[27].

Another interesting aspect of this study was the ability to distinguish between the cell types. The method used was sufficient to identify prespore and prestalk cells at the correct proportions of about 7:3. Our method also reproduced the expected observation that prespore cells are more synchronous than prestalk cells because they are more homogeneous in terms of gene expression and subtypes[25,30]. We did not address the synchronicity levels of the prestalk cell subtypes or the coordination between prespore and prestalk cell synchronicity in this study.

Using scRNA-seq to measure and study cell-level synchronicity during development in other organisms could shed light on this fascinating phenomenon and the developmental disorders that might arise in its absence.

Methods

Vector constructs

The CRISPR vector pO2H_acaAcrispr was constructed by inserting the sgRNA targeting sequence for the *acaA* gene[56] into the backbone vector pDGB_O2H_CRISPR1[57]. The sgRNA sequence was: 5' TCGATCACAC AACAAAGGGG TGG 3' (the last three nucleotides are the Protospacer Adjacent Motif, PAM) To sequence the genomic regions edited by Cas9 in individual clones, we amplified the target region using the following primers: acaA_seq_F1: 5' CAAACAAATG AATTACATGA TGG 3', acaA_-seq_R1: 5' TAATTTGTGA ATTATAATGT TGATG 3'.

To overexpress *pkaC*, we generated the vector pA1H_[coaA]:PkaC-HA. The *pkaC*-HA fragment was amplified from pDXA_PkaC-HA, kindly provided by Dr. Shigenori Hirose, using the following primers: pkaC_ F1_AATG: 5' GCGCCGTCTC ACTCGAATGA GTAACTCAAA TAA-TAATAGC TC 3', and pkaC-HA_ R2_GCTT: 5' GCGCCGTCTC ACTCGAAGCT TAAGCATAAT CTGGAACATC A 3'. We domesticated the fragment into the pUPD2 vector in the GoldenBraid system[58]. We also amplified a 1.7 kb fragment from AX4 genomic DNA containing the *coaA* promoter using the following primers: coaAp_F1_GGAG: 5' GCGCCGTCTC ACTCGGGAGTT AAACAAACAT TATCTTCAAG AC 3', and coaAp_R2_AATG: 5' GCGCCGTCTC ACTCGCATTG TGAAATTAGT TTAAAATACA AATAAAG 3'. We domesticated the fragment into the pUDP2 vector. Subsequently, we assembled the *coaA* promoter, *pkaC*-HA coding sequence, and *mhcA* terminator into the pDGB_A1H backbone vector in a single GoldenBraid assembly step[58]. The plasmids pO2H_acaAcrispr (plasmid ID 1103) and pA1H_[coaA]:PkaC-HA (plasmid ID 1104) are available from the Dicty Stock Center.

Strain construction

All the *D. discoideum* strains were derivatives of AX4[59]. Strains tagged with genes encoding different fluorescent protein markers were used to distinguish between the pooled biological replicates. The mNeonGreen strain was generated by transforming AX4 with the plasmid pDGB_O1N_[act15]:mNeonGreen[58]. The other fluorescent AX4 strains were generated previously as indicated in Table 1. The fluorescently labeled *acaA*$^-$ strains were generated by transforming the fluorescent derivatives of AX4 with the CRISPR vector pO2H_acaAcrispr and the *acaA* mutation was validated by PCR amplification and sequencing of the targeted region. To generate the *acaA*$^-$*pkaC*^{OE} strain, the *acaA*$^-$ mCherry strain was transformed with the expression vector pA1H_[coaA]:PkaC-HA by electroporation.

Cell growth, development, and collection

All the strains were cultured in HL5 medium (5 gr/L Bacto Protease Peptone No:2, Gibco #212120; 5 gr/L Bacto Protease Peptone No:3, Gibco #211693; 5gr/L Proteose Peptone, Millipore #1072291000; 7 gr/L Bacto Yeast Extract Gibco #212720; 1.5 gr/L KH_2PO_4, Fisher BioReagent #BP362; 0.5 gr/L Na_2HPO_4, Fisher BioReagent #BP332; 10 gr/L Dextrose, Fisher BioReagent #D16; 0.5 gr/L Streptomycin sulfate, Sigma Aldrich # S6501; 0.1 gr/L Penicillin G, Sigma Aldrich #P3032; 0.6 mg/L Vitamin B_{12}

Table 1 | Strains used in this study

Strain name	Description	Parental strain	Antibiotic resistance	References
AX4(DBS0235552)[a]	Laboratory wild type, axenic	NC4	N/A	Knecht et al.[59]
AX4 mCherry	Constitutive expression of mCherry under act15 promoter	AX4	G418	Katoh-Kurasawa et al.[12]
AX4 mCerulean	Constitutive expression of mCerulean under act15 promoter	AX4	G418	Katoh-Kurasawa et al.[12]
AX4 GFP	Constitutive expression of GFP under act15 promoter	AX4	G418	Benabentos et al.[66]
AX4 mNeonGreen	Constitutive expression of mNeonGreen under act15 promoter	AX4	G418	This study
acaA$^-$ mCherry	Deletion of a single G at 416 bp of the *acaA* coding region, generated by CRISPR/Cas9 mutagenesis	AX4 mCherry	G418	This study
acaA$^-$ mCerulean	Deletion of a single G at 416 bp of the *acaA* coding region, generated by CRISPR/Cas9 mutagenesis	AX4 mCerulean	G418	This study
acaA$^-$ GFP	Deletion of a single G at 416 bp of the *acaA* coding region, generated by CRISPR/Cas9 mutagenesis	AX4 GFP	G418	This study
acaA$^-$ mNeonGreen	Deletion of a single G at 416 bp of the *acaA* coding region, generated by CRISPR/Cas9 mutagenesis	AX4 mNeonGreen	G418	This study
acaA$^-$*pkaC*^{OE} mCherry	Constitutive expression of PkaC-HA under coaA promoter	*acaA*$^-$ mCherry	G418, Hyg	This study

[a]Dictyostelium Stock Center strain number DBS0235552.

(Cyanocobalamin), Sigma Aldrich #V2876; 0.2 mg/L Folic Acid, Sigma Aldrich #F8758; pH 6.5), supplemented as indicated in Table 1, at 22 °C in shaking suspension. To develop the AX4 and *acaA*$^-$ strains, 2.8×10^7 cells from each strain were harvested during exponential growth, washed with 20 mM potassium phosphate buffer (KK2, pH6.4), and deposited in pure populations on a 47 mm diameter, 0.45 µm pore size, membrane filter placed on top of an absorbent pad (Cytiva Whatman™, Cat No. 7153-104). The cells were developed at 22 °C in a humid chamber and samples were collected at four-hour intervals up to 20 h. Multicellular structures after the tight aggregate stage were harvested as the retained fraction after passage through a 70 µm nylon cell strainer (Falcon®, REF 352350) and dissociated into single cells in KK2 containing 20 mM EDTA and 25 µg/ml Actinomycin D, as described[60]. Single cells were collected as the flowthrough fraction after filtration through a 40 µm nylon cell strainer (Falcon®, REF 352340). We pooled equal numbers of cells from 3 to 4 different tagged strains at each time point, washed the cells 2–3 times by centrifugation at 350 x *g* for three minutes and resuspension in KK2, and immediately processed for single-cell RNA-seq. For the *acaA*$^-$*pkaC*^{OE} strain, 8.4×10^7–1.0×10^8 cells were developed as above in three independent replicates and processed separately. The higher cell density (6.7–8.0×10^6 cells/cm^2 as opposed to 2.2×10^6 cells/cm^2 for AX4 and *acaA*$^-$) compensates for the reduced ability of *acaA*$^-$*pkaC*^{OE} cells to aggregate across long distances by cAMP chemotaxis[24].

Single-cell RNA-sequencing

Single-cell gene expression libraries were prepared using the Chromium Single Cell Gene Expression 3v3.1 or 3v4 kits (10x Genomics). Briefly, single cells, reverse transcription (RT) reagents, Gel Beads containing barcoded oligonucleotides, and oil were loaded onto a Chromium X instrument (10x Genomics) to generate Gel Beads-In-Emulsions (GEMs). Within each GEM, full-length cDNA was synthesized and uniquely barcoded for each individual cell. After GEMs disruption, cDNAs from individual cells were pooled, purified using Dynabeads MyOne Silane Beads (ThermoFisher Scientific #37002D), and amplified by PCR. The amplified products were subsequently fragmented to optimal sizes, followed by end-repair, A-tailing, and adaptor ligation. Final libraries were generated through a second round of amplification.

Following quality control, the libraries were sequenced on the NovaSeq 6000 or NovaSeq X platforms (Illumina), yielding an average of 387 million paired-end 150 bp reads per library. Across 30 libraries, a total of approximately 11.6 billion reads were acquired. Raw sequencing data in FASTQ format were processed using Cell Ranger Count pipeline (v7.2.0 or v8.0.1) on the 10x Genomics Cloud Analysis platform. Reads were aligned to a custom *Dictyostelium* genome reference that included the 4 fluorescent reporter genes, using default parameters for alignment, barcode assignment, and UMI counting.

Data analysis

Quality control and outlier detection. To identify potentially aberrant cells, we applied a robust quality control procedure based on the median absolute deviation (MAD) to each sample[61]. First, we calculated several quality control measures: the total number of sequencing-reads per cell (library size), the number of genes detected per cell, the proportion of reads originating from the 20 most highly expressed transcripts, and the fraction of reads mapped to mitochondrial genes. For each of these measures, we determined the sample-wide median and MAD. We flagged cells as potential outliers if their log-transformed library size, log-transformed gene count, or top 20 transcript fraction deviated by more than five MADs from the median. Because damaged or dying cells often exhibit elevated mitochondrial transcripts, we evaluated the mitochondrial read fraction separately. Cells were marked as outliers if their mitochondrial content was either more than three MADs above the median or exceeded an absolute threshold of 20%. All flagged cells were classified as outliers and excluded from further analysis (Supplementary Fig. 3a).

Cell embedding with foundation model. All cells were embedded using the four-layer version of the Universal Cell Embedding (UCE) method[27]. This transformer-based model generated a 1280-dimensional representation of each cell. We used pretrained model weights that were originally trained primarily on mammalian data. Since the model accepts protein sequences as input, it is not limited to any one species. This property allowed us to generate meaningful representations for *D. discoideum* without additional training, a process known as zero-shot embedding. We then projected these cell representations into two dimensions using Uniform Manifold Approximation and Projection (UMAP)[62] and grouped them into clusters using the Leiden clustering algorithm[63]. Clusters with transcript counts higher than twofold or lower than the median were considered low-quality and removed from further analysis (Supplementary Fig. 3a).

Fluorescent tag scoring and assignment. To perform biological replications for the AX4 and *acaA*$^-$ strains, we generated strains that expressed genes for fluorescent protein markers. Tag assignment was based on the mRNA abundance of the markers. We used GFP, mCerulean, and mCherry for AX4, and GFP, mCerulean, mCherry, and mNeonGreen for *acaA*$^-$. We log-transformed the raw expression values, and excluded zero values (indicating no detectable expression) from further analysis. For each marker, we estimated the distribution of

expression intensities using Gaussian kernel density estimation. Then, we identified peaks in the distribution and used the first peak (lowest intensity) as a threshold to distinguish signal from background. If no peak was identified, we used the 99th percentile of the expression values as a fallback threshold. We adjusted all the thresholds by subtracting the smallest value, so that the minimum threshold started at zero. Each cell was assigned a tag-specific score calculated as its log-expression minus the shift. The tag with the highest positive score was assigned to that cell. If none of the scores were positive, the cell was labeled as "Unassigned" (Supplementary Fig. 3b).

Cell type classification. We defined cells as either prespore or prestalk by applying Leiden clustering to the cell embeddings at 12, 16, and 20 h. The clusters were annotated as prespore or prestalk based on the expression of known marker genes (see Supplementary Table 4). Supplementary Fig. 3c shows these gene expression data as a heat map.

Temporal synchronicity analysis and confidence intervals. To quantify cellular synchronicity, we first calculated the average pairwise Euclidean distance between all cell embeddings at each time point and then averaged these distances (Supplementary Fig. 3d). Because the embeddings were L2-normalized (i.e., each vector had a unit length), the maximum possible distance between any two cells is 2. We used this property to define a normalized synchronicity score, where higher values reflect greater similarity (and thus higher synchronicity) among cells:

$$Synchronicity(t) = \frac{1}{N}\sum_{u,v}\frac{2 - d(u,v)}{2}$$

Here, $d(u,v)$ is the distance between a pair of cells, and N is the total number of unique cell pairs at time t. Synchronicity scores range from 0 (completely dissimilar) to 1 (identical).

To estimate confidence intervals, we applied a nonparametric bootstrap at the replicate level. We resampled the replicate-level synchronicity scores with replacement 10,000 times, computed the mean for each resample, and took the 2.5th and 97.5th percentiles of this distribution as the 95% confidence bounds (Fig. 2 and Supplementary Fig. 1). Differences between groups were assessed using t-tests on the replicate-level means (Supplementary Tables 1, 2, 3, 5, 6, and 7).

Principal component analysis

To verify that our conclusions did not depend on the UCE method, and to provide a conservative, widely used baseline for comparison, we repeated the analysis using PCA. We combined the data from all cells of the three strains into a single dataset, normalized total counts per cell, and log-transformed the values. We then computed the first 50 principal components on this combined dataset, L2-normalized the resulting cell vectors, and calculated synchronicity using the same Euclidean-distance-based formula as for the UCE embeddings. The resulting trajectories and confidence intervals were computed in the same way as for the UCE-based analysis.

Statistics and reproducibility

Statistical methods are described in the context of each method used. Sample size, the number of replicates, and the definition of replicates are included in the results section and in the figure legends. The issue of replication is also addressed specifically in Supplementary Fig. 2, as well as the corresponding results, discussion, and methods sections of the main text.

Reporting summary

Further information on research design is available in the Nature Portfolio Reporting Summary linked to this article.

Data availability

Raw sequencing reads and processed data have been deposited in the NCBI Gene Expression Omnibus (GEO) under accession number GSE305468. It is available from Zenodo with the DOI 10.5281/zenodo.18481907[64]. The numerical source data underlying the graphs are available in Supplementary Data 1 (Fig. 2); Supplementary Data 2 (Supplementary Fig. 1); and Supplementary Data 3 (Supplementary Fig. 2a and Fig. 2). All other data and materials are available from the corresponding author on reasonable request.

Code availability

Custom code and reproducible workflows are available at https://github.com/lenatr99/scRNA_dicty, including pipelines for 10x preprocessing, UCE embeddings, UMAP/Leiden clustering, fluorescent-tag assignment, prespore/prestalk classification, synchronicity scoring with bootstrap confidence intervals, and figure generation. The repository includes step-by-step instructions and environment files to enable full reproducibility. It is available from Zenodo with the DOI 10.5281/zenodo.18481808[65].

Received: 1 October 2025; Accepted: 23 February 2026;
Published online: 06 March 2026

References

1. Oates, A. C., Morelli, L. G. & Ares, S. Patterning embryos with oscillations: structure, function and dynamics of the vertebrate segmentation clock. *Development* **139**, 625–639 (2012).
2. Lee, J. D. & Treisman, J. E. In *Drosophila Eye Development. Results and Problems in Cell Differentiation* (ed K. Moses) Vol. 37 (Springer, 2002).
3. Spudich, J. A. *Dictyostelium discoideum: molecular approaches to cell biology* (Academic Press, 1987).
4. Kessin, R. H. *Dictyostelium - Evolution, cell biology, and the development of multicellularity* (Cambridge University Press, 2001).
5. Hall, A. L., Schlein, A. & Condeelis, J. Relationship of pseudopod extension to chemotactic hormone-induced actin polymerization in amoeboid cells. *J. Cell Biochem.* **37**, 285–299 (1988).
6. Loomis, W. F. *Dictyostelium discoideum. A developmental system* (Academic Press, 1975).
7. Kriebel, P. W., Barr, V. A. & Parent, C. A. Adenylyl cyclase localization regulates streaming during chemotaxis. *Cell* **112**, 549–560 (2003).
8. Sgro, A. E. et al. From intracellular signaling to population oscillations: bridging size- and time-scales in collective behavior. *Mol. Syst. Biol.* **11**, 779 (2015).
9. Brock, D. A. et al. A Dictystelium mutant with defective aggregate size determination. *Development* **122**, 2569–2578 (1996).
10. Artemenko, Y., Lampert, T. J. & Devreotes, P. N. Moving towards a paradigm: common mechanisms of chemotactic signaling in Dictyostelium and mammalian leukocytes. *Cell. Mol. Life Sci.* **71**, 3711–3747 (2014).
11. Antolovic, V., Lenn, T., Miermont, A. & Chubb, J. R. Transition state dynamics during a stochastic fate choice. *Development* **146**. https://doi.org/10.1242/dev.173740 (2019).
12. Katoh-Kurasawa, M. et al. Transcriptional milestones in Dictyostelium development. *Genome Res.* **31**, 1498–1511 (2021).
13. Parikh, A. et al. Conserved developmental transcriptomes in evolutionarily divergent species. *Genome Biol.* **11**, R35 (2010).
14. Rosengarten, R. D. et al. Leaps and lulls in the developmental transcriptome of Dictyostelium discoideum. *BMC Genom.* **16**, 294 (2015).
15. Van Driessche, N. et al. Global transcriptional responses to cisplatin in Dictyostelium discoideum identify potential drug targets. *Proc. Natl. Acad. Sci. USA* **104**, 15406–15411 (2007).
16. Van Driessche, N. et al. A transcriptional profile of multicellular development in Dictyostelium discoideum. *Development* **129**, 1543–1552 (2002).
17. Westbrook, E. R., Lenn, T., Chubb, J. R. & Antolovic, V. Collective signalling drives rapid jumping between cell states. *Development* **150**. https://doi.org/10.1242/dev.201946 (2023).

18. Kim, J., Heslop-Harrison, P., Postlethwaite, I. & Bates, D. G. Stochastic noise and synchronisation during dictyostelium aggregation make cAMP oscillations robust. *PLoS Comput. Biol.* **3**, e218 (2007).
19. Laub, M. T. & Loomis, W. F. A molecular network that produces spontaneous oscillations in excitable cells of Dictyostelium. *Mol. Biol. Cell* **9**, 3521–3532 (1998).
20. Siegert, F. & Weijer, C. Digital image processing of optical density wave propagation in Dictyostelium discoideum and analysis of the effects of caffeine and ammonia. *J. Cell Sci.* **93**, 325–335 (1989).
21. Brimson, C. A. et al. Collective oscillatory signaling in Dictyostelium discoideum acts as a developmental timer initiated by weak coupling of a noisy pulsatile signal. *Dev. Cell* **60**, 918–933.e914 (2025).
22. Cai, H. et al. Nucleocytoplasmic shuttling of a GATA transcription factor functions as a development timer. *Science* **343**, 1249531 (2014).
23. Pitt, G. S. et al. Structurally distinct and stage-specific adenylyl cyclase genes play different roles in Dictyostelium development. *Cell* **69**, 305–315 (1992).
24. Wang, B. & Kuspa, A. Dictyostelium development in the absence of cAMP. *Science* **277**, 251–254 (1997).
25. Jermyn, K. A., Duffy, K. T. & Williams, J. G. A new anatomy of the prestalk zone in Dictyostelium. *Nature* **340**, 144–146 (1989).
26. Sternfeld, J. & David, C. N. Fate and regulation of anterior-like cells in Dictyostelium slugs. *Dev. Biol.* **93**, 111–118 (1982).
27. Rosen, Y. et al. Universal cell embeddings: a foundation model for cell biology. *bioRxiv* https://doi.org/10.1101/2023.11.28.568918 (2024).
28. Eder, M. et al. Systematic mapping of organism-scale gene-regulatory networks in aging using population asynchrony. *Cell* **187**, 3919–3935.e3919 (2024).
29. Martinez-Jimenez, C. P. et al. Aging increases cell-to-cell transcriptional variability upon immune stimulation. *Science* **355**, 1433–1436 (2017).
30. Maeda, M. et al. Changing patterns of gene expression in dictyostelium prestalk cell subtypes recognized by in situ hybridization with genes from microarray analyses. *Eukaryot Cell* **2**, 627–637 (2003).
31. Do, V. H. & Canzar, S. A generalization of t-SNE and UMAP to single-cell multimodal omics. *Genome Biol.* **22**, 130 (2021).
32. Yang, Y. et al. Dimensionality reduction by UMAP reinforces sample heterogeneity analysis in bulk transcriptomic data. *Cell Rep.* **36**, 109442 (2021).
33. Salvidge, W. M. et al. Linage priming and cell type proportioning depends on the interplay between stochastic and deterministic factors. *eLife* **14**, RP105512 (2025).
34. Iranfar, N., Fuller, D. & Loomis, W. F. Transcriptional regulation of post-aggregation genes in Dictyostelium by a feed-forward loop involving GBF and LagC. *Dev. Biol.* **290**, 460–469 (2006).
35. Corrigan, A. M. & Chubb, J. R. Regulation of transcriptional bursting by a naturally oscillating signal. *Curr. Biol.* **24**, 205–211 (2014).
36. Chen, G., Shaulsky, G. & Kuspa, A. Tissue-specific G1-phase cell-cycle arrest prior to terminal differentiation in Dictyostelium. *Development* **131**, 2619–2630 (2004).
37. Shaulsky, G. & Loomis, W. F. Mitochondrial DNA replication but no nuclear DNA replication during development of Dictyostelium. *Proc. Natl. Acad. Sci. USA* **92**, 5660–5663 (1995).
38. Singer, G., Araki, T. & Weijer, C. J. Oscillatory cAMP cell-cell signalling persists during multicellular Dictyostelium development. *Commun. Biol.* **2**, 139 (2019).
39. Hashimura, H., Morimoto, Y. V., Yasui, M. & Ueda, M. Collective cell migration of Dictyostelium without cAMP oscillations at multicellular stages. *Commun. Biol.* **2**, 34 (2019).
40. Hirose, S., Katoh-Kurasawa, M. & Shaulsky, G. Cyclic AMP is dispensable for allorecognition in Dictyostelium cells overexpressing PKA-C. *J. Cell Sci.* **134**. https://doi.org/10.1242/jcs.258777 (2021).
41. Hirose, S., Chen, G., Kuspa, A. & Shaulsky, G. The polymorphic proteins TgrB1 and TgrC1 function as a ligand-receptor pair in Dictyostelium allorecognition. *J. Cell Sci.* **130**, 4002–4012 (2017).
42. Kay, R. R. & Thompson, C. R. L. Cross-induction of cell types in Dictyostelium: evidence that DIF-1 is made by prespore cells. *Development* **128**, 4959–4966 (2001).
43. Thompson, C. R. & Kay, R. R. The role of DIF-1 signaling in Dictyostelium development. *Mol. Cell* **6**, 1509–1514 (2000).
44. Richardson, D. L., Loomis, W. F. & Kimmel, A. R. Progression of an inductive signal activates sporulation in Dictyostelium discoideum. *Development* **120**, 2891–2900 (1994).
45. Shaulsky, G., Kuspa, A. & Loomis, W. F. A multidrug resistance transporter/serine protease gene is required for prestalk specialization in Dictyostelium. *Genes Dev.* **9**, 1111–1122 (1995).
46. Chen, Z. H. & Schaap, P. Secreted cyclic Di-GMP induces stalk cell differentiation in the eukaryote dictyostelium discoideum. *J. Bacteriol.* **198**, 27–31 (2016).
47. Consalvo, K. M. et al. Extracellular signaling in Dictyostelium. *Int. J. Dev. Biol.* **63**, 395–405 (2019).
48. Yoshino, R. et al. Regulation of ammonia homeostasis by the ammonium transporter AmtA in Dictyostelium discoideum. *Eukaryot Cell* **6**, 2419–2428 (2007).
49. Chen, X. et al. Terpene synthase genes in eukaryotes beyond plants and fungi: Occurrence in social amoebae. *Proc. Natl. Acad. Sci. USA* **113**, 12132–12137 (2016).
50. Chen, X. et al. Diversity and functional evolution of terpene synthases in dictyostelid social amoebae. *Sci. Rep.* **8**, 14361 (2018).
51. Chen, X. et al. A terpene synthase-cytochrome P450 cluster in Dictyostelium discoideum produces a novel trisnorsesquiterpene. *Elife* **8**. https://doi.org/10.7554/eLife.44352 (2019).
52. Loomis, W. F. Role of PKA in the timing of developmental events in Dictyostelium cells. *Microbiol. Mol. Biol. Rev.* **62**, 684–694 (1998).
53. Schaap, P. From environmental sensing to developmental control: cognitive evolution in dictyostelid social amoebas. *Philos. Trans. R Soc. Lond. B Biol. Sci.* **376**, 20190756 (2021).
54. Warren, J. & Kumar, J. P. Patterning of the Drosophila retina by the morphogenetic furrow. *Front. Cell Dev. Biol.* **11**, 1151348 (2023).
55. Hirose, S., Santhanam, B., Katoh-Kurosawa, M., Shaulsky, G. & Kuspa, A. Allorecognition, via TgrB1 and TgrC1, mediates the transition from unicellularity to multicellularity in the social amoeba Dictyostelium discoideum. *Development* **142**, 3561–3570 (2015).
56. Sekine, R., Kawata, T. & Muramoto, T. CRISPR/Cas9 mediated targeting of multiple genes in Dictyostelium. *Sci. Rep.* **8**, 8471 (2018).
57. Lehmann, P., Katoh-Kurasawa, M., Kundert, P. & Shaulsky, G. Going against the family: perturbation of a greenbeard pathway leads to falsebeard cheating. *iScience* **27**, 111125 (2024).
58. Kundert, P. et al. A GoldenBraid cloning system for synthetic biology in social amoebae. *Nucleic Acids Res.* **48**, 4139–4146 (2020).
59. Knecht, D. A., Cohen, S. M., Loomis, W. F. & Lodish, H. F. Developmental regulation of Dictyostelium discoideum actin gene fusions carried on low-copy and high-copy transformation vectors. *Mol. Cell Biol.* **6**, 3973–3983 (1986).
60. Katoh, M. et al. An orderly retreat: Dedifferentiation is a regulated process. *Proc. Natl. Acad. Sci. USA* **101**, 7005–7010 (2004).
61. Luecken, M. D. & Theis, F. J. Current best practices in single-cell RNA-seq analysis: a tutorial. *Mol. Syst. Biol.* **15**, e8746 (2019).
62. McInnes, L., Healy, J., Saul, N. & Großberger, L. UMAP: uniform manifold approximation and projection. *J. Open Sour. Softw.* **3**. https://doi.org/10.21105/joss.00861 (2018).
63. Traag, V. A., Waltman, L. & van Eck, N. J. From Louvain to Leiden: guaranteeing well-connected communities. *Sci. Rep.* **9**, 5233 (2019).
64. Katoh-Kurasawa, M., Shaulsky, G., Trnovec, L. & Zupan, B. Filtered single cell RNA sequencing AnnData objects for Dictyostelium developmental synchronicity study (AX4, acaA, acaA pkaC) (v1.0.0) [Data set]. Zenodo. https://doi.org/10.5281/zenodo.18481907 (2026).

65. Trnovec, L. scRNA-seq analysis pipeline for dictyostelium developmental synchronicity (v1.0.0). Zenodo. https://doi.org/10.5281/zenodo.18481808 (2026).
66. Benabentos, R. et al. Polymorphic members of the lag gene family mediate kin discrimination in Dictyostelium. *Curr. Biol.* **19**, 567–572 (2009).

Acknowledgements

This research was supported by the National Science Foundation (grant number 2319686) through the Integrative Organismal Systems program, as well as by the Slovenian Research and Innovation Agency (grants numbers L2-60154 and P2-0209).

Author contributions

G.S. conceived the study. G.S., R.C., and M.K.-K. designed the experiments. M.K.-K. performed most of the experiments and data collection, with additional data collected by P.L. and sample processing assistance from Y.L. L.T. led the data analysis and software development, with contributions from M.K.-K. and close guidance from B.Z. G.S. wrote the manuscript. All authors revised and edited the manuscript. G.S., R.C. and B.Z. supervised the project. M.K.-K. and L.T. contributed equally to this work. G.S. and B.Z. jointly oversaw key aspects of the research.

Competing interests

The authors declare no competing interests.

Additional information

Supplementary information The online version contains supplementary material available at https://doi.org/10.1038/s42003-026-09806-5.

Correspondence and requests for materials should be addressed to Blaž. Zupan or Gad Shaulsky.

Peer review information *Communications Biology* thanks the anonymous reviewers for their contribution to the peer review of this work. Primary Handling Editors: David Favero and Rosie Bunton-Stasyshyn. A peer review file is available.